THE ASTROPHYSICAL JOURNAL, 473:294–303, 1996 December 10

PROPERTIES OF LOW-MASS OBJECTS IN NGC 2024

F. COMERÓN,[1,2] G. H. RIEKE,[3,4] AND M. J. RIEKE[3]

Received 1995 June 30; accepted 1996 June 26

ABSTRACT

We have obtained deep *JHK* imaging of the central region of the NGC 2024 embedded cluster, allowing three-color measurements of 151 sources. We show that contamination by background sources is small, and we reject a small number of sources that are probably foreground. We use a Monte Carlo isochrone fitting technique to estimate the luminosities and masses of the low-mass members of the embedded cluster. We find that the IMF between ~ 0.04 and $\sim 0.5\ M_\odot$ can be fitted within the errors with a power law of slope -1.2 in linear mass units (or -0.2 in logarithmic units). There is no indication of a turnover of the IMF at the bottom of the main sequence; it appears to continue down to $\sim 0.04\ M_\odot$ with no significant deviation (within our moderately large errors) from the power law. This estimate of the IMF includes only the primary members of binary (or multiple) systems. Of a subset of 35 sources, 24 (69%) appear to have infrared excesses indicating possible circumstellar disks, supporting arguments that disk formation is not inhibited in high-density clusters.

Subject headings: H II regions — ISM: individual (NGC 2024) — open clusters and associations: individual (NGC 2024) — stars: low-mass, brown dwarfs — stars: luminosity function, mass function

1. INTRODUCTION

The Orion complex is the most thoroughly studied star-forming region (Goudis 1982; Genzel & Stutzki 1989). Unlike more nearby sites of star formation like Taurus-Auriga and ρ Ophiuchi, where only low-mass stars are being formed at present, Orion displays simultaneous ongoing star formation at all stellar masses (Zinnecker, McCaughrean, & Wilking 1993). It is therefore an ideal site to extend measurements of the initial mass function over a broad range of masses.

The NGC 2024 H II region is one of the most conspicuous features of the Orion complex. It is located in the Orion B (=L1630) giant molecular cloud (Maddalena et al. 1986), near its interface with the *b* subgroup of the Orion OB1 association (Blaauw 1964). Under the hypothesis that star formation in the Orion OB1 association is propagating from the *a* to *d* subgroups (Elmegreen & Lada 1977; Blaauw 1991), star formation in NGC 2024 would have been triggered by activity in the neighboring *b* subgroup, whose nuclear age is estimated at 5×10^6 yr (Warren & Hesser 1978).

The structure of the H II region and its associated molecular material have been discussed in detail by Barnes et al. (1989), who also found a cluster of about 30 infrared point sources. A more extensive survey enabled Lada et al. (1991b) to discover many more faint members of the NGC 2024 cluster in their study of the global star formation in the Orion B cloud. These studies suggest that NGC 2024 is an excellent site to study the low-mass IMF: (1) it is at relatively high Galactic latitude and contains a very dense infrared cluster, which stands out clearly compared with the density of background sources; (2) the large column density of molecular material provides a nearly opaque screen that further reduces the degree of background contamination; and (3) the large number of sources allows the embedded cluster to be studied with good statistics.

In this paper, we present the results of a new, deep near-infrared survey of NGC 2024 in the *J*, *H*, and *K* bands, which samples most of the area covered by the embedded cluster. The infrared photometry of the sources is analyzed by fitting models of young stars and substellar objects to determine the mass function. Our analysis is based on a technique developed in a previous study of the ρ Ophiuchi cluster (Comerón et al. 1993, hereafter CRBR, and described further in Williams et al. 1995). The sensitivity of our survey should allow us to detect massive substellar objects in the cluster; at the age of NGC 2024, these sources should still be in a stage of deuterium burning that provides a brief interval of stable energy output before they begin to fade permanently from sight. Our results will be compared to those obtained applying the same technique to the ρ Oph cluster.

2. OBSERVATIONS AND DATA REDUCTION

Observations were carried out in 1993 October 23–26, with the Steward Observatory 2.3 m telescope, using a NICMOS3 256 × 256 HgCdTe array in a camera that provides a scale of 0.″64 per pixel. Frames were taken in the *J* (1.25 μm), *H* (1.65 μm), and *K* (2.2 μm) bands. Each frame was constructed from a set of 16 short exposures, with small telescope motions between exposures to allow for efficient flat-fielding and bad pixel removal. A flat field is constructed by median averaging the set of exposures of a given field, rejecting the highest and lowest values of a given pixel to eliminate stars and cosmic rays. Exposure times for individual exposures were 30 s for both the *H* and *K* bands and 90 s for the *J* band.

The fields were selected from the *K*-band mosaic published by Lada et al. (1991b). So far as possible, regions with bright nebulosity were avoided, and where portions of our frames were contaminated by nebulosity, we discarded these regions from further analysis. A total of five fields was imaged with some overlap among them, so that the area covered by our survey is approximately 30 square arcmin. Figure 1 displays the limits of this area.

[1] Departament d'Astronomia i Meteorologia, Universitat de Barcelona, 08028 Barcelona, Spain.
[2] Currently at European Southern Observatory.
[3] Steward Observatory, University of Arizona, Tucson, AZ 85721.
[4] Department of Planetary Sciences, University of Arizona, Tucson, AZ 85721.

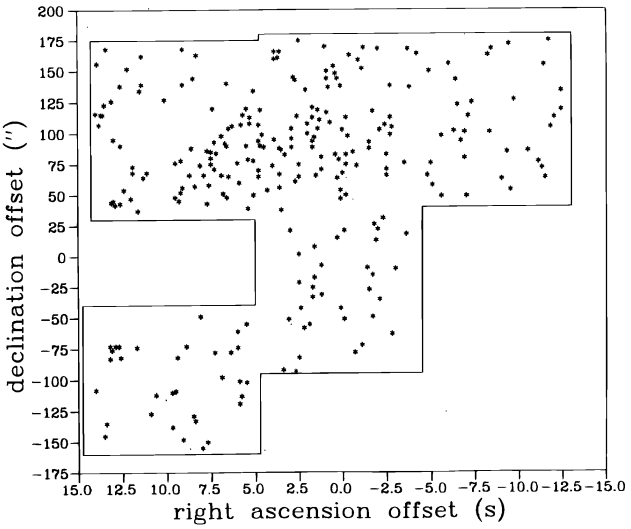

FIG. 1.—Map of the surveyed area of NGC 2024, showing the positions of the sources detected in 2 μm. The offsets are referred to the position $\alpha = 5^h39^m5^s.0$, $\delta = -1°56'30''$ (equinox 1950.0).

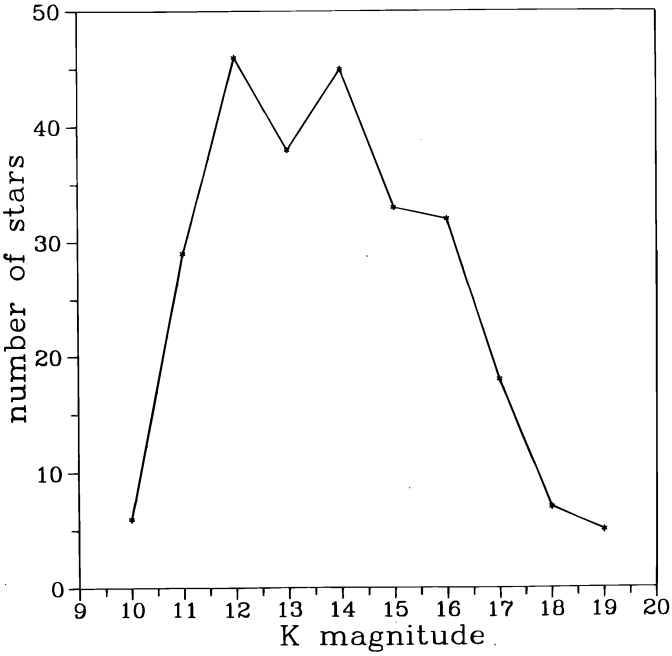

FIG. 2.—Histogram of apparent K magnitudes. The completeness limit is at about $m_k = 17$.

Reduction of the frames was performed under the IRAF image analysis software. Astrometry was performed with the DAOFIND task and with positional references from the 2 μm survey of Barnes et al. (1989). These positions are in good agreement with those derived by offsetting the telescope from SAO 132444 and using the pixel scale given above. We estimate the overall positional accuracy to be better than 3".

Photometry of the array images was carried out using the PHOT task under IRAF and calibrated by means of observations of the *JHK* standard stars HD 22686 and HD 40335 (Elias et al. 1982). The task parameters were optimized to avoid contamination of the measurements due to the crowdedness of the field, leading to selection of a 5".1 aperture for the source and an annulus of 9".0 and 10".9 inner and outer diameters for sky. We verified that our

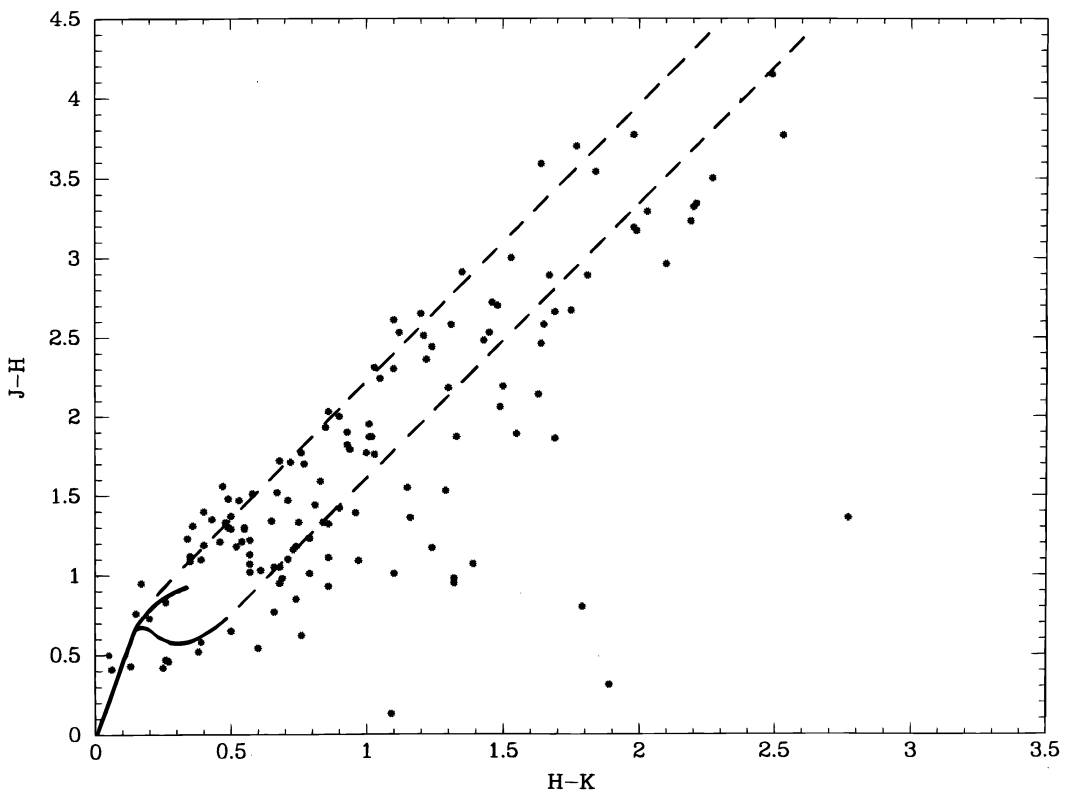

FIG. 3.—($J-K$, $H-K$) diagram for all the sources detected in J, H, and K. The sources lying at very small values of $J-K$ for their $H-K$ color are all very faint, and their position in this color-color diagram very probably is caused by erroneous magnitude measurements.

results were not sensitive to reasonable changes in these parameters. The rms photometric accuracy in each band is estimated to be better than 10%, except for very faint sources near the visibility limit where the uncertainties can be somewhat larger. The completeness magnitude is not uniform through all the frames as a consequence of faint local nebulosities that may make faint sources fall below the detection limit. As a result, we cannot verify completeness by obtaining a deeper image for part of the field as we did for ρ Oph. However, from comparison with this previous work (CRBR), we estimate the completeness limits over most of the surveyed field to be $m_J \simeq 19.5$, $m_H \simeq 18.5$, $m_K \simeq 17$. A total of 261 sources was detected in K, 213 in H, and 152 in J. All sources detected in J were detected in H and, with the exception of one source near the detection limit in both J and H, all sources detected in H were detected in K.

Figure 2 shows a histogram of the K magnitudes in the surveyed area. Stars brighter than $m_K \simeq 9.5$ are missing because they tend to be surrounded by bright nebulosity and therefore were excluded from our survey. Our histogram is similar to those of Lada et al. (1991b) and Hodapp (1994), with the distribution peaking near $m_K \simeq 12$. Lada et al. attributed this peak to the incompleteness of their survey for stars fainter than $m_K \simeq 13$. However, our survey and that of Hodapp have significantly fainter limits, showing that the peak at $m_K \simeq 12$ is a real feature of the apparent luminosity function of the cluster; this behavior is very similar to the result of McCaughrean & Stauffer (1994) for the Trapezium cluster. A color-color diagram is presented in Figure 3.

3. DATA ANALYSIS

3.1. *Basic Method*

At the age of an embedded cluster, young, low-mass stars are still contracting toward the main sequence, invalidating the application of main-sequence relationships among mass, luminosity, and the effective temperature. Time-dependent models of early stellar and substellar evolution (D'Antona & Mazzitelli 1985, 1994; Nelson, Rappaport, & Joss, 1986; Laughlin & Bodenheimer 1993; Burrows et al. 1993) are required to interpret the infrared observations. The models predict the evolution of luminosity and temperature for a given mass; these parameters can be compared to the measured magnitudes and colors. This comparison has to take into account the wavelength-dependent obscuration by the intervening dust, spectral features in the atmosphere of the star, and the possible existence of circumstellar disks.

The procedure followed by us to fit the models to the observations is described in detail in CRBR and in Williams et al. (1995). In summary, the age of a source is assumed to be known (see discussion below), and a trial temperature is chosen for the fit. Assuming the object has no infrared excess due to circumstellar emission, the intrinsic colors of the object are assumed to be determined uniquely by the temperature through the Planckian behavior corrected for the (temperature-dependent) atmospheric features in each band. Given the theoretical isochrone, the temperature corresponds to a luminosity (or equivalently an absolute bolometric magnitude). With the bolometric magnitude and theoretical colors as boundary conditions, we attempt a fit to the observed colors correcting for extinction. The fit is optimized by adjusting the trial temperature (and accompanying bolometric magnitude) and the extinction. There are essentially two unknowns, the temperature and the extinction in one of the bands; the rest of the parameters are given by the stellar models and the extinction law. Thus, in principle, measurements in two colors would suffice to fit the source properties. In general, we require at least three colors as a check on the underlying assumptions and on the presence of infrared excesses. The residuals in a least-squares fit to the three-color photometry determine whether the model satisfactorily reproduces the observations. Through the theoretical models, this best fit provides the mass of the object.

3.2. *Infrared Excesses*

In general, the embedded sources will have varying degrees of infrared excess. Adams, Lada, & Shu (1987) use the spectral index $n = d \log (\lambda f_\lambda)/d \log \lambda$ to distinguish general types of source. Class I sources ($n > 0$) are interpreted as protostars whose luminosity is dominated by accretion of infalling material onto a central, immersed object. Class II sources ($0 > n > -2$) are taken to be T Tauri stars surrounded by a nebular disk responsible for the infrared excess of the source, either by reprocessing the short-wavelength emission of the central object or by producing energy from the infall of matter onto it. Finally, class III sources ($-2 > n > -3$) are believed to be the central object after dispersal of the nebular disk.

Given the limited wavelength coverage of our JHK photometry, we have tentatively taken all sources with $H - K > 3.5$ to be class I (including those detected only at K with $M_K < 14$). As discussed below, these sources constitute no more than 6% of those detected in our survey. Class I sources are not modeled adequately by our method; if instead these sources were very heavily obscured class II or III sources, they would be added to the high-luminosity, high-mass counts and would have little effect on the low-mass IMF which is the focus of this paper. We therefore do not include them in our analysis.

As in CRBR, we fit colors of sources of class II and III in a way that approximately reproduces the theoretical spectral energy distributions. This fit assumes the emission is dominated by the photosphere up to the peak of the spectral energy distribution, and that for longer wavelengths there is a power-law excess expressed as a magnitude difference Δm_λ with respect to the blackbody law. For NGC 2024, where we have only J, H, K, photometry, this approach is equivalent to identifying class II sources as ones which are fitted adequately at J and H but which show a modest excess at K compared with class III ones. For stars with temperature above $\sim$4500 K, the J, H, K bands no longer sample the spectrum adequately to determine a temperature. Therefore, we have ignored the details for stars best fitted by masses above 2 $M_\odot$, simply treating them as "high-mass" stars.

3.3. *Source Models*

For masses below 0.2 $M_\odot$, we have used the models of Burrows et al. (1993). The mass range below 0.2 $M_\odot$ has also been studied by D'Antona & Mazzitelli (1994). Some discrepancies in the stellar models still persist due to differences in the input physics, but to first order these issues are understood (see discussion in Burrows et al. 1993 and D'Antona & Mazzatelli 1994). In this mass range, the differences between the models of D'Antona & Mazzitelli and

Burrows et al. arise largely from the different treatment of the atmosphere. A discussion of the effects of an incomplete atmospheric model on the location of the pre–main-sequence tracks in the luminosity-temperature diagram can be found in Burrows et al. We have selected their tracks in our analyses in the low-mass and substellar range because of the more detailed treatment of the atmosphere than in D'Antona & Mazzitelli. The uncertainties in our observational analysis appear to be dominated by uncertainties in the ages of the embedded sources rather than by the likely errors in these models.

We have used the tracks of D'Antona & Mazzitelli (1994) above 0.2 $M_\odot$. The differences among different sets of models in this mass range are relatively small. To ensure a smooth merging with the models used for $M < 0.2\,M_\odot$, we have taken the results listed in Tables 3 and 7 of D'Antona & Mazzitelli. These models are based on Alexander, Augason, & Johnson (1989) and Rodgers & Iglesias (1992) opacities and MLT convection. Although choosing another set of isochrones, with different convection and opacity parameters, would result in measurable differences in luminosity and temperature, such differences are small compared to the uncertainties in our analysis due to age effects.

The spectral energy distribution in the infrared for objects with temperatures above $\sim$3500 K is reasonably well approximated by that of a blackbody. At lower temperatures, absorptions due to neutral and low-ionization-potential species and to molecules become important. In this range, we have computed corrections to the blackbody fluxes based on the atmosphere models by Allard & Hauschildt (1995), which include most important atomic and molecular species. Although these models are likely to underestimate the fluxes at H and K for our objects, as shown by those authors, the agreement is satisfactory within our photometric accuracy.

3.4. *Foreground Extinction*

We have used the extinction law of Rieke & Lebofsky (1985). Although the extinction in star forming regions at blue and visible wavelengths is known to vary from the standard law, such variations are small in the infrared (Rieke & Lebofsky 1985; Clayton & Mathis 1988).

4. RESULTS AND DISCUSSION

Most distance determinations to NGC 2024 are consistent with a distance modulus of 8.1 to the Orion B cloud, equivalent to a distance of 415 pc, as found by Anthony-Twarog (1982) from narrow band photometry of B stars. We have adopted this value for the present study.

4.1. *Background, Foreground, and Interloper Contamination*

Because of the proximity of NGC 2024, its small spatial extent, its angular separation from the galactic plane, and the obscuration of the background sources by the molecular cloud, we expect that nearly all of the infrared sources detected in our survey are physically related to the cluster.

We have estimated the potential contamination by foreground stars using the model of Jones et al. (1981) of the Galactic K luminosity function. In the direction $b = -17°$ of NGC 2024, and up to a distance of 415 pc, one would expect to see some 440 stars per square degree brighter than $m_K = 17$ and with spectral type M5 or earlier. Due to the steepening of the luminosity-mass relationship at the faint end, later type M dwarfs would only slightly increase this count. Scaled to the 30 square arcmin of our survey, we would expect to find three to four foreground sources earlier than M5 V (i.e., with $m_K \leq 14.5$) and a smaller number of fainter ones. We have found five likely foreground sources, identified by their relatively blue colors ($H - K < 0.3$). These sources have been excluded from our further analyses.

Background contamination is mainly due to red giants at large distances from the galactic plane; it is decreased by the dimming of background stars by the dust in the molecular cloud. The average extinction due to the NGC 2024 cloud can be evaluated from the ^{13}CO observations of Bally, Langer, & Liu (1991), who found velocity-integrated line intensities of up to 60 K km s^{-1} along some lines of sight. Adopting 45 K km s^{-1} as an average value, and the calibration of 1 K km s^{-1} $\rightarrow A_V = 1$ mag derived by Bally et al. for the excitation conditions of Orion, we estimate $A_V = 45$ mag for the average background extinction. Using the Rieke & Lebofsky (1985) extinction law, this translates to $A_K \simeq 5.0$ mag. The unobscured K magnitude for background sources still to be above our detection limit should therefore be $m_K = 12$ or brighter; from Jones et al.'s (1981) models, the expected number of such sources in the direction of Orion is about 175 per square degree, or only one to two in our whole survey. However, the assumption of a uniform background extinction usually underestimates the number of background sources, as in a clumpy cloud a good part of the contamination comes from faint background sources observed through extinction "holes." Comerón, Torra, & Rieke (1996) have estimated the required correction to take into account the clumpiness of the cloud; in the case of a cloud at the latitude of NGC 2024, and assuming a typical clump mass spectral index $\alpha = -1.6$, the above estimate for the number of background sources should be multiplied by a factor of less than 2, still making it insignificant. Other derivations of the extinction in NGC 2024 (Mezger et al. 1988) tend to give higher values than the one adopted by us. On the other hand, a few areas of our survey probably have extinctions below the mean value; even with generous assumptions about these areas, no more than $\sim$5% of the detected sources can arise from the background.

Finally, we can estimate the probability of finding a star accidentally lying in the region occupied by NGC 2024 but having no physical relation to it. Again, the most likely type for such an interloper is an early M dwarf. Taking the density of stars of all types earlier than M5 at the position of Orion according to the parameters of Jones et al. (1981), and assuming a depth of the NGC 2024 cluster of $\sim$0.6 pc (similar to its size in the plane of the sky), the probability of finding an interloper in the sampled volume is less than 1%.

4.2. *Class I Sources*

Two of our sources are very close to the positions of the far-infrared sources FIR 1 and FIR 3 studied by Mezger et al. (1988). Their positions, colors and magnitudes are given in Table 1. The color indices would imply extinctions $A_V >$ 50 mag if they arose from extinction by intervening dust, and they are possible class I sources with strong infrared excesses. Mezger et al. estimate a mass of $\simeq 15\,M_\odot$ for FIR 1 and $\simeq 50\,M_\odot$ for FIR 3, suggesting that they are protostellar cores which may ultimately give rise to intermediate- or high-mass stars. In addition to the maxima corresponding to FIR 1 and FIR 3, we have found four more near-

TABLE 1

SOURCES IDENTIFIED IN 1300 μm AND NH_3 SURVEYS

Number	α (1950)	δ (1950)	J	H	K	Remarks
1.....	$5^h39^m10^s.1$	$-1°55'12''$		17.6	14.1	FIR 1
2.....	5 39 10.9	−1 55 30	17.1	14.0	11.8	
3.....	5 39 11.6	−1 55 42		19.2	15.4	FIR 3
4.....	5 39 12.3	−1 55 19		15.4	13.7	
5.....	5 39 13.9	−1 57 43	12.0	11.5	11.4	IRS 22 (Barnes et al. 1989)
6.....	5 39 12.3	−1 54 57	17.6	14.5	12.3	

infrared sources within 5″ of NH_3 peaks in the survey of Gaume, Johnston, & Wilson (1992). The positions and magnitudes of these sources are also given in Table 1. These additional sources are moderately red, probably early T Tauri stars still associated with remnants of their protostellar envelopes, with the exception of source number 5, which is associated with a visible star. Additional possible class I sources ($H - K > 3.5$) are located along the obscuring dust bar where the sources of Mezger et al. lie. In total, we find 13 candidate class I sources.

4.3. *Disk Properties*

To address the isue of the decay time of circumstellar disks in the NGC 2024 cluster, we have used the lowest mass objects detected in our survey. Deuterium burning in the early contraction of objects with masses below 0.2 $M_\odot$ stabilizes the temperature and luminosity temporarily, giving origin to a "deuterium-burning main sequence" (Burrows et al. 1993). The duration of this stable stage is comparable to the upper limit to the age of the NGC 2024 cluster. Therefore, in this mass range we obtain a unique solution for the extinction and the intrinsic infrared excess. We have found 35 sources measured in all three colors for which these arguments apply. We find that 24 of these objects are of class II, with detectable excesses, and the remaining of class III, with little or no excess. Despite the relatively high density of the NGC 2024 forming cluster, it appears that a large portion of its members have excesses possibly resulting from circumstellar disks.

We have performed the same fit with ρ Oph data of CRBR, obtaining six sources with $n > -2$ out of 17 objects fitted by masses below 0.2 $M_\odot$ (only slightly different from the result of six out of 16 obtained from Table 4 of CRBR from fits based on the pre–main-sequence tracks of D'Antona & Mazzitelli 1985). Thus, within the statistics, the fractions of low-mass stars with circumstellar disks in the two clusters are similar, but there is a hint of a lower proportion in ρ Oph. If the difference in the counts is real, it would indicate either a longer lifetime of disks or a younger age of NGC 2024 as compared to ρ Oph. For ρ Oph, Wilking, Lada, & Young (1989) estimated an age of 3.5×10^6 yr or less, and a duration of the T Tauri phase of 1.5×10^6 yr, in agreement with the relative proportions found by us. Assuming that the T Tauri phase has the same duration in NGC 2024 as in ρ Oph, we thus derive an age of $\simeq 2 \times 10^6$ yr for NGC 2024, well below the upper limit quoted in the introduction. Recent infrared spectroscopy (Greene & Meyer 1995) suggests a much younger age for ρ Oph than the upper limit of Wilking et al. (1989), in which case the disk incidence in NGC 2024 would lead us to make its age less than 2×10^6 yr; in the following we will adopt 1×10^6 yr as a working assumption.

4.4. *The Initial Mass Function*

As we have outlined above, fitting the photometry of an embedded object requires choosing an isochrone. Usually a range of isochrones gives an acceptable fit, each predicting a different age and mass for the object. In view of the resulting uncertainties for individual sources, we have adopted a statistical approach to the problem of determining the mass function. We adopt a maximum age for the cluster. We then construct a table for each object containing the model parameters resulting from fits to different isochrones up to this maximum age. If, for a given isochrone, the required amount of extinction is positive and the mean residual for the best-fitting temperature is consistent with the measurement errors, then that isochrone is considered to give a possible age for the star. Entries are made in the table at age intervals of 2.5×10^5 yr. A possible apparent mass function is obtained by randomly choosing the mass corresponding to one of the possible values of the age for every star. This procedure is repeated many times to determine the most likely apparent mass function and the uncertainties resulting from the lack of knowledge of the ages of the individual stars.

This method is different from that used by CRBR, where only two isochrones were considered, the choice depending on whether or not the best fit was obtained with or without an infrared excess. The procedure we have applied here has the advantage of a more relaxed constraint on the range of possible ages for the members of the cluster, by depending only on an upper limit to those ages.

Simulations of this Monte Carlo fitting technique demonstrate that the age uncertainties for the sources dominate the other sources of error such as those due to the propagation of photometric errors or to uncertainties in the models for low-mass objects. These simulations also show that our approach does not lead to a bias in the assigned masses. Hence, the procedure provides both an unbiased measure of the IMF and also allows us to derive the likely errors.

Our approach makes the implicit assumption that star formation in an embedded cluster occurs over an extended timescale. This assumption agrees with the behavior of young clusters deduced by Lada & Lada (1995). In contrast, Zinnecker et al. (1993) and Strom, Edwards, & Skrutskie (1993) assume coeval star formation when using theoretical isochrones to derive the shapes of the absolute magnitude functions in clusters. Thus, the typical star-forming history of a young cluster must be considered to be poorly understood. To test our approach, we applied the dereddening prescription of Strom et al. (1993) to derive the distribution of absolute J magnitudes for our data. We find a peak around $M_J = 3$ for NGC 2024 and at $M_J = 6$ for ρ Oph, indicating that the ρ Oph cluster may be older than the one in NGC 2024. However, the shapes of the J_0 magnitude

functions cannot be matched by any of the coeval model functions, suggesting a mixture of ages in both clusters.

To constrain the formation rate, we have assumed the end of the protostellar phase (class I to class II transition) to take place at an age of 1.5×10^5 yr, in agreement with both theoretical and observational studies of the birthline for young stars (Cohen & Kuhi 1979; Stahler 1983). Thus, at the 1.5×10^5 yr isochrone, the object is assumed to have a spectral index of $n = 0$. The progressive dispersal of the circumstellar disk is represented by an exponential decay of the spectral index, which asymptotically approaches $n = -3$ with time. In accordance with the results from the preceding section, we assume a disk lifetime of $\frac{2}{3}$ the assumed maximum age of NGC 2024 and $\frac{1}{3}$ that of ρ Oph.

In a magnitude-limited survey like ours, the fraction of the sampled volume of the cloud decreases with decreasing intrinsic luminosity of the embedded objects. The apparent mass function must be corrected for the resulting underestimate of the number density of faint objects to obtain the true mass function. The true number density n of objects within a given range of masses has been calculated on the basis of the method used by Schmidt (1975) for deriving space densities of quasars:

$$n \propto \sum_i \frac{1}{V_i},$$

where V_i is the volume of the cloud where the object would still be detected in our survey. A bias in this derivation can arise by assuming that the cloud is homogeneous. This issue has been discussed by Comerón et al. (1996), who showed that a significant contribution to the counts of intrinsically faint objects (i.e., those with unobscured magnitudes close to the limiting magnitude of the survey) comes from sources seen through regions where a given level of extinction is reached at a greater depth in the cloud, due to the random arrangement of the constituting clumps, rather than from sources located in the forefront of the cloud where the average extinction is low. In a homogeneous cloud, V_i would simply be proportional to the highest extinction that the source i may have and still be included in the survey; however, when correcting for clumpiness, V_i is larger than the value for homogeneous cloud with the same value of the highest extinction. To correct for the clumpiness, we used a mass spectrum index $\alpha = -1.5$ (Lada, Bally, & Stark 1991) in the formalism of Comerón et al. (1996) and with an average background extinction $A_K = 5$ mag.

Our results for the completeness-corrected IMF are presented in Figure 4*a*. The error bars represent the quadratic sum of two contributions: (1) the scatter in each bin obtained from the Monte Carlo computation of different isochrone choices; and (2) the square root of the average number of stars in each bin. There are additional sources of error which are difficult to estimate quantitatively, such as the accuracy of the family of isochrones used in our calculations and of the completeness corrections. Both of these uncertainties will affect the lowest mass bin most strongly. However, even if we reduced the counts in this bin by a factor of 2, our data would be consistent with a smooth variation of the IMF across the stellar/substellar boundary, with a power-law fit that would be approximately flat in logarithmic units.

The different curves shown in Figure 4*a* correspond to different assumed maximum ages of the stellar population, ranging from 5×10^5 yr to the upper limit of 5×10^6 yr. It is apparent that the derived shape of the mass function in NGC 2024 depends on the assumed age. These trends are qualitatively as expected. For example, the derived number density of very low mass objects ($M < 0.2\ M_\odot$) is not very sensitive to the assumed age except in the extreme case of 5×10^6 yr, as expected because of the slow evolution of such low-mass objects while they are on the deuterium-burning main sequence. The behavior at higher masses can be explained on similar grounds. For the youngest ages, many bright sources can be fitted as young, not very massive and relatively cool objects. For greater ages, these sources tend to be fitted better by isochrones for more massive and hotter objects, corresponding to the general evolution of young stars as they settle toward the main sequence. Consequently, there is a general tendency for the IMF to become flatter as the assumed cluster age is made greater. Except for the 5×10^6 yr case, however, the derived mass functions are in reasonably good agreement, despite these systematic trends. Both because this age is at the upper limit for this cluster, and because it leads to a bimodal IMF that is unlikely to be realistic, we set it aside. According to the preceding discussion, an age of $\sim 10^6$ yr is probably appropriate; changes in assumed age by factors of 2 in either direction have only a minor effect.

We have used the improved analysis to reconsider our data for ρ Oph. As seen in Figure 4*b*, no significant differences are found among the mass functions for cluster ages of 5×10^5, 10^6 and 2×10^6 yr. Greene & Meyer (1995) have reported infrared spectra of some of the sources in our study of ρ Oph, leading them to assign an age of $\sim 5 \times 10^5$ yr to the embedded cluster. As summarized in CRBR, previous studies in the optical led to an upper limit of 3.5×10^6 yr. Therefore, over the plausible age range the derived mass function is not significantly changed. Greene & Meyer also assigned significantly lower masses to some of the sources CRBR assigned intermediate masses. The change in masses is primarily a result of the younger age (Williams et al. 1995). As Figure 4*b* illustrates, although assigning a younger age will tend to reduce the derived masses as a group, the effect of age uncertainties on the slope of the calculated IMF is relatively small.

Approximating the number density of objects in NGC 2024 by a power law, $n(M)dM \propto M^\alpha dM$, we find $\alpha \simeq -1.2 \pm 0.1$. This slope is consistent with that found for ρ Oph, in the same mass range, $\alpha \simeq -1.4 \pm 0.2$. In logarithmic mass units, the corresponding values are $\alpha \simeq -0.2 \pm 0.1$ and $\alpha \simeq -0.4 \pm 0.2$, respectively. For both clusters, the lowest mass bin containing massive brown dwarfs has the largest uncertainties, due to the corrections for completeness and the higher sensitivity to background contamination. Therefore, we cannot provide a more detailed analysis of the shape of the low-mass IMF beyond these power-law fits.

Values of $\alpha \sim -1$ for the slope of the low-mass IMF are also found in well-studied cluster such as the Hyades, Pleiades, and Praesepe (Hambly, Hawkins, & Jameson 1991; Hambly et al. 1995; Laughlin & Bodenheimer 1993; Leggett et al. 1994; Williams et al. 1996). The field mass function also seems to have $\alpha \sim -1$ without evidence for a turnover at the lowest masses (Kroupa, Tout, & Gilmore 1990, 1993; Tinney, Mould, & Reid 1992; Jarrett, Dickman, & Herbst 1994). Our extension of this slope into the substellar range in both ρ Oph and NGC 2024 implies that,

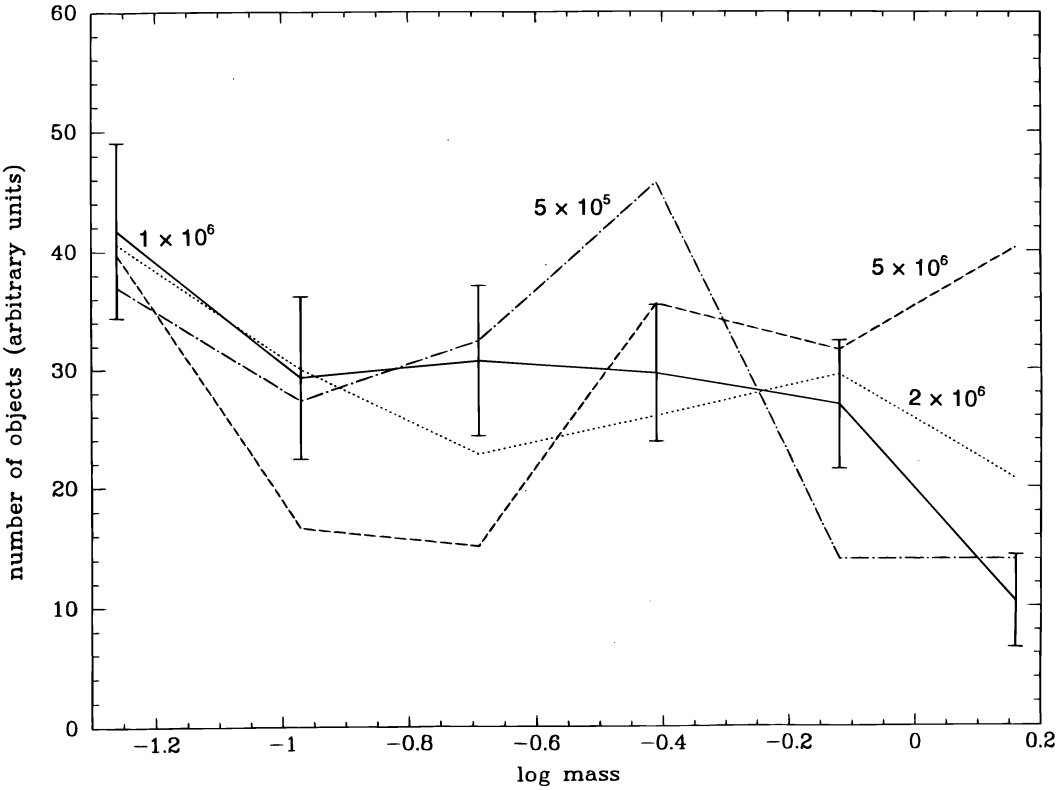

FIG. 4*a*

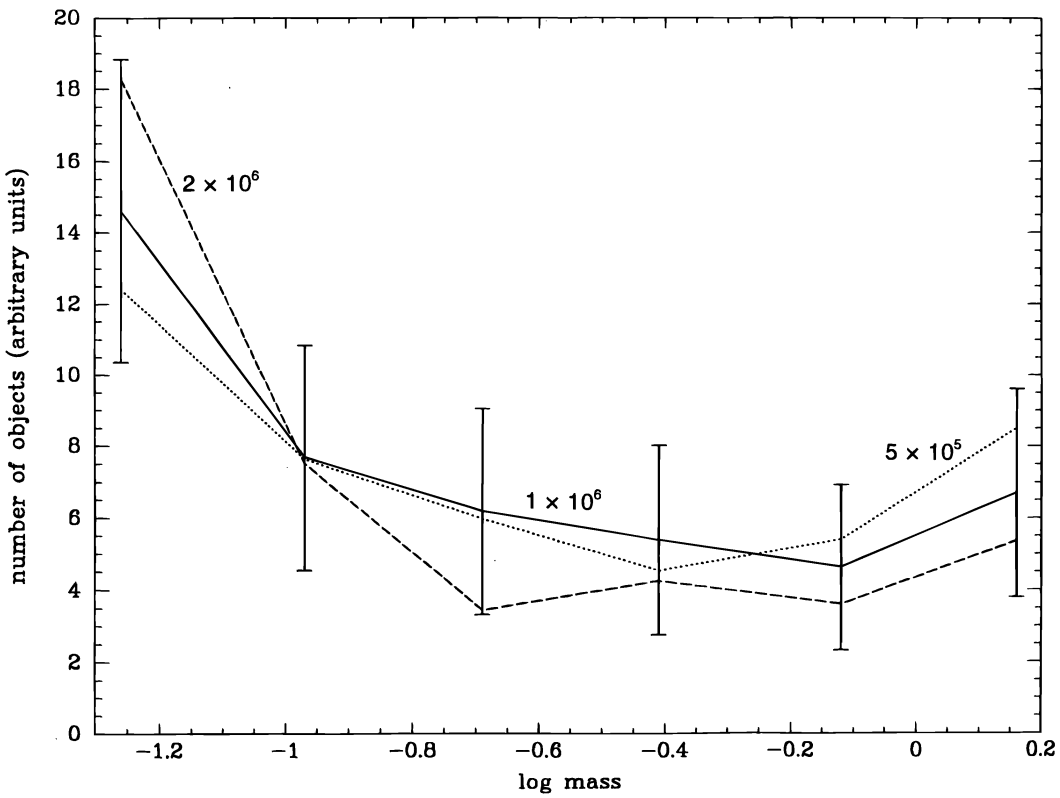

FIG. 4*b*

FIG. 4.—(*a*) Mass function of the NGC 2024 cluster. The dot-dashed, solid, dotted, and dashed lines refer, respectively, to assumed maximum cluster ages of 5×10^5, 1×10^6, 2×10^6, and 5×10^6 yr. Error bars are plotted only for an age of 10^6 yr, but are similar for all the curves. (*b*) Mass function of the ρ Oph cluster. The dotted, solid, and dashed lines refer, respectively, to assumed maximum cluster ages of 5×10^5, 1×10^6, and 2×10^6 yr. Error bars are plotted only for an age of 10^6 yr, but are similar for all the curves.

although they make only a small contribution to the total mass, massive brown dwarfs must be abundant in open clusters and probably also in the field.

4.5. *Possible Biases*

To ensure that the derived low-mass IMF in NGC 2024 is not influenced by an improper correction for completeness, we have computed the mass function with no completeness correction and with a correction which assumed that the cloud is homogeneous rather than clumpy. These two assumptions bracket the real behavior of a clumpy cloud. We find that the derived space density of objects in the low-mass bin ($0.04\ M_\odot < M < 0.08\ M_\odot$) decreases by about 20% when the completeness correction is neglected. On the other hand, a completeness correction assuming a homogeneous cloud produces only a slight increase ($\simeq 5\%$) in the derived space density of very low mass objects. It appears that the completness correction has a rather weak influence on the derived shape of the mass function for the lowest mass objects.

The derivation of the low-mass end of the mass function may also be sensitive to small amounts of background contamination. In regions where the column density of the cloud is overestimated, background sources might be difficult to distinguish from low-mass cluster members. We have recalculated the mass function of the cluster, rejecting the sources appearing in the northwestern field of the survey where the molecular measurements suggest the extinction is lower than the average. Our results now show a small decrease in the number of stars below $0.3\ M_\odot$ relative to higher mass objects. However, the overall effects on the derived IMF is small and well within the quoted error bars.

Undetected binariety of cluster members may modify the derived mass function in several ways. For example, if one of the members of a binary system is much brighter than the other, the flux at each band is dominated by the luminous one, and the fit simply ignores the existence of the faint one. In the opposite extreme where both members have similar temperature and luminosity, they would be moved upward in the color-magnitude diagrams and would be considered to be a single, more luminous and more massive object. Because of these complications, we have applied our fitting procedure to simulated samples of binary stars with different masses of the primary and mass ratios. These simulations show that the error in the mass derived neglecting binariety is always much less than that resulting from uncertainties in the age.

It is difficult to quantify the potential contamination by the faint members of undetectable binaries on the derived mass function, as the distribution of mass ratios in binary systems is rather poorly known (Duquennoy & Mayor 1991; Mazeh et al. 1992). Therefore, the mass function we present should be considered to include only the primary stars in binary systems. However, if the mass function of the secondaries is identical to that of the primaries, then the overall IMF is affected only near inflections. To the extent a simple power law is an adequate fit to our data, low-mass secondaries would have little influence on the shape of the IMF (but they would affect its normalization).

It has been suggested that accretion of the circumstellar disk or envelope by a central class II young stellar object may still substantially increase its mass before the circumstellar material is finally dispersed. In that case, the masses we derive would represent only a lower limit to the final mass of the object. Circumstellar masses of class I and II objects in ρ Oph have been derived by André & Montmerle (1994) based on the flux reemitted by cold dust at 1.3 mm. Ten low-mass class II sources for which stellar masses were derived by CRBR are included, all of which have circumstellar masses of $0.01\ M_\odot$ or less. The highest circumstellar-to-stellar mass ration for the sources detected by André & Montmerle is only 6%. They conclude that young stellar objects have already incorporated nearly all of their masses at the end of the class I stage. Further accretion of circumstellar material is unlikely to alter the mass function of the currently observed class II and class III sources in NGC 2024.

In summary, we do not believe that the slope of the mass function of NGC 2024 can be affected strongly by an erroneous assumed age or completeness correction, to background contamination, to binariety of the cluster members, or that it represents a temporary state that will change after accretion has run its course for the cluster members.

4.6. *X-Ray Properties*

The intense coronal activity of young stars is revealed by their X-ray emission, which suffers relatively mild attenuation by foreground material and hence provides a check of the influence of extinction on the results from other wavelengths.

Recent X-ray observations of NGC 2024 are reported by Freyberg & Schmitt (1995). Of the 52 sources they detect, 23 are in the area surveyed by us. For 21 of these sources, we find plausible infrared counterparts within 15″ of the X-ray position (with the exception of their number 18 which lies 22″ from a possible identification). Object 10 is detected only in the K band, and is fainter than our completeness limit. Object 39 is identified with IRS 2, a star excluded from our survey because of its brightness. The only object detected by *ROSAT* without a possible near-infrared counterpart is number 13, which is the fifth brightest object in their survey.

Most of the X-ray sources have intermediate masses and luminosities, out of the range where our method for deriving physical parameters works best. Nevertheless, we can obtain rough estimates for the luminosities that are useful to study the global X-ray properties of the cluster. Two sources, however (numbers 30 and 40), have luminosities too high to be estimated and have been excluded from further consideration.

To determine the intrinsic properties of the X-ray sources, we must determine the extinction in this energy domain. The proportionality factor between A_J and A_X is expected to be a function of the level of extinction and the spectra of the sources because of the large variation in extinction level across the broad *ROSAT* passband. We have analyzed the behavior of the X-ray and J-band fluxes from the embedded sources in NGC 2024 to find $A_X \sim 0.6A_J$, in excellent agreement with the relation obtained by Casanova et al. (1995) for large values of extinction (i.e., $A_V > 10$), as is the case for most of our sources. Deviations from this extinction law are expected to be small, as shown by Ride & Walker (1977) and Morrison & McCammon (1983).

We set $A_X = 0.6A_J$ to analyze the properties of the sources. We then found a relatively constant value of $L_X/L_{\rm bol} \sim 10^{-3.5}$ for young objects with near-solar luminosities in NGC 2024. This is in good agreement with the

results of Feigelson et al. (1993) and Casanova et al. (1995) for Chamaeleon I and ρ Oph, and is consistent with the ratio found by Strom & Strom (1994) for sources in L1495 E with similar luminosity. Therefore, the X-ray properties of the embedded sources appear to be consistent with the properties derived by our isochrone fitting procedure.

4.7. *The Clump and Stellar Mass Functions*

Comparison of the mass function for gas clumps in a cloud and the derived stellar mass function may provide information on the instabilities and fragmentation processes leading to the buildup of the stellar mass function. Although the molecular core associated with the NGC 2024 cluster has not been resolved (Lada et al. 1991a), observations of other clouds at a higher spatial resolution show clumpiness to be present at all length scales (Blitz 1993), with a distribution of masses given by a spectral index in linear mass units of -1.5 for $M > 1\ M_\odot$ (Blitz 1993). However, most such studies do not extend to very low clump masses. Pound & Blitz (1995) have searched the ρ Oph cloud for self-gravitating clumps between 0.01 and 10 $M_\odot$. They find a flat spectrum, i.e., spectral index in linear mass units of -1, which appears to apply from 0.01 to ~ 5 $M_\odot$.

Details of the clump mass spectrum are poorly determined in the study of Pound & Blitz because it is based on a total of only 13 clumps and may suffer from incompleteness for the lowest mass clumps. However, as they point out, it appears not to be in good agreement with the stellar IMF, which has a slope of -1 from 0.08 to $\sim 0.6\ M_\odot$ and then steepens to a slope of -2.5 above this mass. Where the discrepancy lies depends on where one normalizes the two mass functions. If they are normalized at high masses, then low-mass objects are underrepresented in the clump spectrum. Pound & Blitz normalize by integrated mass, which is virtually equivalent (the four most massive clumps account for 82% of the total clump mass), and they deduce such a discrepancy. However, if the clump spectrum is normalized at low masses, then the discrepancy is an excess of high-mass clumps. Furthermore, assuming incompleteness is not a problem, the clump mass spectrum slope agrees roughly with that for the low-mass stellar (and substellar) IMF, whereas above $\sim 0.6\ M_\odot$ the clump spectrum is much shallower than any estimates of the IMF.

A very simple model discussed by Zinnecker et al. (1993) assumes that every clump gives rise to a star whose mass M_* is proportional to a power p of the clump mass $M_{\rm cl}$, $M_* \propto M_{\rm cl}^p$. If the stellar mass function and the clump mass function have the forms $N_* dM \propto M^{-x} dM$ and $N_{\rm cl} dM \propto M^{-y} dM$, respectively, this implies

$$x = \frac{y - 1 + p}{p}\ .$$

A value of $p < 1$ might then reproduce the slope of the stellar mass function at high masses, where $x > y$. That is, in this model the more massive clumps lose a substantial portion of their mass in the process of collapsing into stars. However, the index $x \simeq 1$ found by us for low-mass stars both in ρ Oph and NGC 2024 suggests that they grow by accretion without significant loss of mass from the original clump. Alternately, the high-mass clumps may fragment and contribute to the low-mass IMF.

4.8. *Star Formation Efficiency*

The star-formation efficiency in NGC 2024 can be determined using the mass function we have derived. We assume a cluster age of 10^6 yr and estimate the total number of stars in the bins of the mass function displayed in Figure 4*a*. In this way, we obtain about 170 stars with $0.06\ M_\odot < M < 2\ M_\odot$ (note that this value is higher than the number of stars actually detected because the mass function has been corrected for incompleteness). Next, we assume a Miller & Scalo (1979) mass function for the higher masses, which allows us to derive a total stellar mass of $\sim 180\ M_\odot$ in the surveyed area. This number must be increased to take into account the bright areas excluded from the survey, leading to a total stellar mass of $200\ M_\odot$ or more.

The mass in gas has been estimated to be $1200\ M_\odot$ by Mezger et al. (1992) from measurements of the emission by cold dust. From a CS survey, Lada et al. (1991a) obtained a virial mass for the cloud of $550\ M_\odot$. As a consequence of the observational uncertainties in both the gas and stellar mass, it is not possible to give an accurate determination of the star-formation efficiency; from the above values, however, we estimate it to be at least 20% and possibly as high as 40%, consistent with the 30% derived by Lada (1992). The star-formation efficiency should reach an even higher value in the future if star formation continues at a comparable rate to that maintained over the last 10^6 yr, which amounts to $10^{-4}\ M_\odot\ {\rm yr}^{-1}$ converted into stars over the whole cluster. Particularly if star formation continues, it is possible that a bound cluster will be left after dispersal of the parental molecular gas, assuming the internal velocity dispersion to be ~ 2 km s^{-1} as in the Trapezium cluster (Jones & Walker 1988).

5. CONCLUSIONS

We have obtained deep J, H, K images of the embedded young cluster in NGC 2024 and fitted its members with theoretical evolutionary models to determine the initial mass function at low masses. We find the following.

1. The low-mass IMF has a power-law slope of $\sim -1.2 \pm 0.1$ in linear mass units (or $\sim -0.2 \pm 0.1$ in logarithmic units). The IMF has no inflection at the bottom of the main sequence; NGC 2024 seems to be forming brown dwarfs at the rate predicted by extrapolating from the slope of the stellar IMF. (Note that the IMF we derive refers to the single stars and to the primary stars of binary pairs.)
2. There are no significant differences between the mass functions in NGC 2024 and ρ Oph.
3. Roughly two-thirds of the low-mass objects in NGC 2024 display infrared excesses characteristic of circumstellar disks.
4. The star-formation efficiency in NGC 2024 up to the present time is at least 20% and perhaps as high as 40%. It is likely to be even higher by the time star formation ceases, possibly leading to the formation of a bound open cluster.

We thank F. Allard and A. Burrows for communicating their theoretical results and for helpful discussions, the anonymous referee for many helpful suggestions that improved the final version of this paper, and the copy editor for assistance with the references. This work was supported

by the NATO Collaborative Research Grants Programme, by the US National Science Foundation, and by NASA grant NAGW-4083 under the Origin of Solar Systems Program. The work of F. C. was also supported by a grant of the CIRIT, and by the CICYT under contracts PB91-0857 and ESP93-1020-E.

REFERENCES

Adams, F. C., Lada, C. J., & Shu, F. H. 1987, ApJ, 312, 788
Alexander, D. R., Augason, G. C., & Johnson, H. R. 1989, ApJ, 345, 1014
Allard, F., & Hauschildt, P. H. 1995, ApJ, 445, 433
André, P., & Montmerle, T. 1994, ApJ, 420, 837
Anthony-Twarog, B. J. 1982, AJ, 87, 1213
Bally J., Langer W. D., & Liu, W. 1991, ApJ, 383, 645
Barnes, P. J., Crutcher, R. M., Bieging, J. H., Storey, J. W. V., & Willner, S. P. 1989, ApJ, 342, 883
Blaauw, A. 1964, ARA&A, 2, 213
Blaauw, A. 1991, in The Physics of Star Formation and Early Stellar Evolution, ed. C. J. Lada & N. D. Kilafis (Dordrecht: Reidel), 125
Blitz, L. 1993, in Protostars and Planets III, ed. E. H. Levy & J. I. Lunine (Tucson: Univ. Arizona Press), 125
Burrows, A., Hubbard, W. B., Saumon, D., & Lunine, J. I. 1993, ApJ, 406, 158
Casanova, S., Montmerle, T., Feigelson, E. D., & André, P. 1995, ApJ, 439, 752
Clayton, G. C., & Mathis, J. S. 1988, ApJ, 327, 911
Cohen, M., & Kuhi, L. V. 1979, ApJS, 41, 743
Comerón F., Rieke, G. H., Burrows, A., & Rieke, M. J. 1993, ApJ, 416, 185 (CRBR)
Comerón, F., Torra, J., & Rieke, G. H. 1996, A&A, 308, 565
D'Antona, F., & Mazzitelli, I. 1985, ApJ, 296, 502
———. 1994, ApJS, 90, 467
Duquennoy, A., & Mayor, M. 1991, A&A, 248, 485
Elias, J. H., Frogel, J. A., Matthews, K., & Neugebauer, G. 1982, AJ, 87, 1029
Elmegreen, B. G., & Lada, C. J. 1977, ApJ, 214, 725
Feigelson, E. D., Casanova, S., Montmerle, T., & Guibert, J. 1993, ApJ, 416, 623
Freyberg, M. J., & Schmitt, J. H. M. M. 1995, A&A, 296, 21
Gaume, R. A., Johnston, K. J., & Wilson, T. L. 1992, ApJ, 388, 489
Genzel, R., & Stutzki, J. 1989, ARA&A, 27, 41
Goudis, C. 1982, The Orion Complex: A Case Study of Interstellar Matter, (Dordrecht: Reidel)
Green, T. P., & Meyer, M. R. 1995, ApJ, 450, 233
Hambly, N. C., Hawkins, M. R. S., & Jameson, R. F. 1991, MNRAS, 253, 1
Hambly, N. C., Steele, I. A., Hawkins, M. R. S., & Jameson, R. F. 1995, MNRAS, 273, 505
Hodapp, K.-W. 1994, ApJS, 94, 615
Jarrett, T. H., Dickman, R. L., & Herbst, W. 1994, ApJ, 424, 852
Jones, B. F., & Walker, M. F. 1988, AJ, 95, 1755
Jones, T. J., Ashley, M., Hyland, A. R., & Ruelas-Mayorga, A. 1981, MNRAS, 197, 413
Kroupa, P., Tout, C. A., & Gilmore, G. 1990, MNRAS, 244, 76
———. 1993, MNRAS, 262, 545
Lada, E. A. 1992, ApJ, 393, L25
Lada, E. A., Bally, J., & Stark, A. A. 1991a, ApJ, 368, 432
Lada, E. A., DePoy, D. L., Evans, N. J., & Gatley, I. 1991b, ApJ, 371, 171
Lada, E. A., & Lada, C. J. 1995, AJ, 109, 1682
Laughlin, G., & Bodenheimer, P. 1993, ApJ, 403, 303
Leggett, S. K., Harris, H. C., & Dahn, C. C. 1994, AJ, 108, 944
Maddalena, R. J., Morris, M., Moscovitz, J., & Thaddeus, P. 1986, ApJ, 303, 375
Mazeh, T., Goldberg, D., Duquennoy, A., & Mayor, A. 1992, ApJ, 401, 265
McCaughrean, M. J., & Stauffer, J. R. 1994, AJ, 108, 382
Mezger, P. G., Chini, R., Kreysa, E., Wink, J. E., & Salter, C. J. 1988, A&A, 191, 44
Mezger, P. G., Sievers, A. W., Haslam, C. G. T., Kreysa, E., Lemke, R., Mauersberger, R., & Wilson, T. L. 1992, A&A, 256, 631
Miller, G. E., & Scalo, J. M. 1979, ApJS, 41, 513
Morrison, R., & McCammon, D. 1983, ApJ, 270, 119
Nelson, L. A., Rappaport, S. A., & Joss, P. C. 1986, ApJ, 311, 226
Pound, M. W., & Blitz, L. 1995, ApJ, 444, 270
Ride, S. K., & Walker, A. B. C. 1977, A&A, 61, 339
Rieke, G. H., & Lebofsky, M. J. 1985, ApJ, 228, 618
Rodgers, F. J., & Iglesias, C. A. 1992, ApJS, 79, 507
Schmidt, M. 1975, ApJ, 202, 22
Stahler, S. W. 1983, ApJ, 274, 822
Strom, K. M., & Strom, S. E. 1994, ApJ, 424, 237
Strom, S. E., Edwards, S., & Skrutskie, M. F. 1993, in Protostars and Planets III, ed. E. H. Levy & J. I. Lunine, (Tucson: Univ. Arizona Press), 837
Tinney, C. G., Mould, J. R., & Reid, I. N. 1992, ApJ, 396, 173
Warren, W. H., & Hesser, J. E. 1978, ApJS, 36, 497
Wilking, B. A., Lada, C. J., & Young, E. T. 1989, ApJ, 340, 823
Williams, D. M., Comerón, F., Rieke, G. H., & Rieke, M. J. 1995, ApJ, 454, 144
Williams, D. M., Boyle, R. P., Morgan, W. T., Rieke, G. H., & Rieke, M. J. 1996, ApJ, 464, 238
Zinnecker, H., McCaughrean, M. J., & Wilking, B. A. 1993, in Protostars and Planets III, ed. E. H. Levy & J. I. Lunine, (Tucson: Univ. Arisona Press), 429